The Influence of a Local Swirl Ratio on Tornado Intensification near the Surface

D. C. LEWELLEN, W. S. LEWELLEN, AND J. XIA

Department of Mechanical and Aerospace Engineering, West Virginia University, Morgantown, West Virginia

(Manuscript received 1 June 1998, in final form 2 March 1999)

ABSTRACT

The results of high-resolution, fully three-dimensional, unsteady simulations of the interaction of a tornado with the surface are presented. The goal is to explore some of the range of structures that should be expected to occur in nature within the tornadic ''corner flow''—that region where the central vortex meets the surface. The most important physical variables considered are the tornado-scale circulation and horizontal convergence, the effective surface roughness, the tornado translation speed, the low-level inflow structure, and the upper-core structure. A key ingredient of the corner flow dynamics is the radial influx of fluid in the surface layer with low angular momentum relative to that of the fluid in the main vortex above it. This low swirl fluid arises initially from outside or below the larger-scale vortex or through frictional loss of angular momentum to the surface and forms much of the vortex core flow after it exits the corner flow region. Changes in the surface layer inflow or upper-core structure can dramatically affect the level of intensification and turbulent structure in the corner flow even when the swirl ratio of the tornado vortex as a whole is unchanged. The authors define a local corner flow swirl ratio, S_c, based on the total flux of low angular momentum fluid through the corner flow and show that it parameterizes the leading effects on the corner flow of changes to the flow conditions immediately outside of the corner flow. As S_c decreases, the low-level vortex intensity rises to a maximal level where mean swirl velocities near the surface reach 2.5 times the maximum mean swirl velocity aloft; further decreases force a transition to a much weaker low-level tornado vortex. This sensitivity suggests that differences in the near-surface inflow layer may be a critical factor in determining whether an existing supercell low-level mesocyclone spawns a tornado or not.

1. Introduction

Viewing any appreciable sample of the videotape records of actual tornadoes, one is impressed by the wide variety of flows that are evidenced, not only in the range of sizes and intensities, but in the different structures encountered. For example, some tornadoes display thin, relatively smooth, almost elegant single funnels on the ground, while others are composed of many highly turbulent secondary vortices revolving about large central cores. Categorizing and understanding this range of structures has been a long-standing goal of tornado research. Controlled laboratory and numerical experiments of confined tornado-like vortices have produced similar ranges of flow structures when a single parameter such as the swirl angle of the incoming flow is varied. Correlating these studies with actual tornadoes in the field is more problematic; here the flow is highly turbulent, and many physical parameters are involved. More important, physical processes on a broad range of length scales from a few meters in the surface layer to many kilometers on the storm scale are all important and strongly coupled with each other. Consequently one finds in the field that storms with seemingly quite similar structure on the kilometer scale may give rise to tornadoes interacting with the surface with quite different structures, or even to no tornado at all.

In broad caricature we can identify three length scales of direct importance to the tornado structure: the storm scale of tens of kilometers, which ultimately drives the entire flow; the outer tornado scale of a few kilometers in which the flow may be considered a converging, swirling plume;[1] and the inner tornado scale of tens to several hundreds of meters characterizing the tornado core, boundary layer, and corner flow regions of the flow. In this work we focus on the last of these regimes and, in particular, on the tornadic corner flow where the boundary layer flow transitions into the core flow. As the place where the tornado vortex meets the ground,

Corresponding author address: Dr. David C. Lewellen, Department of Mechanical and Aerospace Engineering, West Virginia University, P.O. Box 6106, Morgantown, WV 26506-6106.
E-mail: dlewelle@wvu.edu

[1] The outer tornado scale may be identified with the mesocyclone when the tornado spins up directly from the mesocyclone core; when the tornado is better characterized as a secondary vortex within the mesocyclone, these become distinct scales with the mesocyclone scale lying in between the storm and outer tornado scales.

this region is of particular relevance, typically being the scene of the largest velocities, lowest pressures, sharpest velocity gradients, and greatest damage potential in the entire flow. In concentrating on this part of the flow we knowingly set aside the important question of tornadogenesis on the larger scale, that is, of how the storm-scale flow gives rise to and maintains the swirling, converging plume on the few kilometer scale that makes the occurrence of an intense tornadic vortex possible. Instead, we focus on which properties of the velocity and pressure fields immediately outside of the corner flow region most strongly govern the resulting corner flow structure and on how this dependence might best be parameterized. To do this we consider a larger domain than might seem necessary, imposing a variety of flows on the outer tornado scale as our far-field boundary conditions, in order to achieve a physically reasonable range of flow fields immediately bounding the corner flow.

Some researchers have emphasized an inviscid nature of the corner flow as it provides for a rapid transition between the boundary layer and core flows (e.g., Burggraf et al. 1971; Wilson and Rotunno 1986). Inviscid dynamics may be used to explain part of the transition, but we also expect turbulence to play an important role in the flow dynamics in this region where the tornado vortex interacts with the surface. Lewellen et al. (1997, referred to as LLS97 hereafter) presented a large eddy simulation of turbulent transport in the tornado vortex for one set of physical boundary conditions. The results in the corner flow were shown to be relatively independent of grid resolution and subgrid model modifications (for sufficiently fine grid resolution), providing a strong indication that our simulations are properly resolving the most important turbulent eddies in the corner flow. In the present work we utilize this tool for a number of sets of realistic physical conditions in order to address the sensitivity of the vortex flow structure to changes in a variety of physical parameters. Our goals coincide in part with previous laboratory work using tornado vortex chambers, with the advantage in our numerical study that we can explore a wider range of boundary conditions and physical variations, obtain more detailed velocity and pressure measurements with better control over our averaging procedures, and simulate the flows at the higher Reynolds numbers characteristic of the actual atmospheric flow.

In the following section we present a brief description of the tornadic corner flow, using some of our recent simulation results as illustrations. Previous laboratory (e.g., Ward 1972; Snow 1982; Church et al. 1979) and axisymmetric (Lewellen 1962, 1993; Davies-Jones 1973, 1986) modeling studies have shown that one of the primary variables governing the tornado vortex is the swirl ratio of the flow through the vortex. While particular definitions vary in detail, this amounts to the ratio of a typical swirl velocity to a typical flow-through velocity for the converging, swirling plume of the outer tornado-scale flow. By varying this ratio, a range of distinct behaviors in the vortex corner flow region can be realized; however, a given behavior regime is not uniquely determined by any specific value of this ratio. As we will illustrate, other physical parameters also strongly affect the structure of the central vortex corner flow, so that flows that share the same large-scale swirl ratio can produce different corner flow structures.

In order to better categorize the types of corner flows encountered, we will define a local swirl ratio specific to the inner tornado scale. While it is natural to consider the tornado on the few-kilometer scale as a converging plume with large angular momentum, the surface-corner-core flow itself is better characterized as a low angular momentum jet in a background of roughly constant angular momentum. This is close in spirit to the similarity solutions studied by Long (1958), Burggraf and Foster (1977), and Shtern and Hussain (1993), although they did not include any horizontal convergence of the outer flow as we will here. The corner flow swirl ratio we will define is, in essence, a ratio of typical swirl to flow-through velocities for this body of low angular momentum fluid making up the boundary layer and core regions of the flow. The swirl ratio on the outer tornado scale strongly influences the corner flow swirl ratio, but does not uniquely specify it.

A single dimensionless ratio is certainly inadequate to completely describe the corner flow; nonetheless, we have found that the dominant effects on the corner flow of many physical variables—such as surface roughness, low-level inflow structure, the large-scale swirl ratio, or the properties of the upper core of the vortex—are largely captured by their effects on the corner flow swirl ratio. In section 2 we present examples of tornado vortices exhibiting corner flow behavior characteristic of different swirl ratios and then present a definition for the corner flow swirl ratio. In section 3 we describe our dataset of simulated tornadic vortices under different physical conditions and plot some selected time averaged results from this dataset versus the new swirl ratio. The numerical model and simulation procedures are as described in LLS97 with one addition: a modification of the subgrid model to incorporate rotational damping effects, which is described in the appendix. In section 4 we discuss some important features of the corner flow structure that are only partly governed by the corner flow swirl ratio, in particular, the nature of the turbulent fluctuations and the strength and character of secondary vortices. We close in section 5 with a summary and discussion of future work.

2. A local swirl ratio for categorizing vortex corner flow dynamics

a. Basic corner flow dynamics

In order to simplify the theoretical discussion of the interaction of the tornado vortex with the surface, as

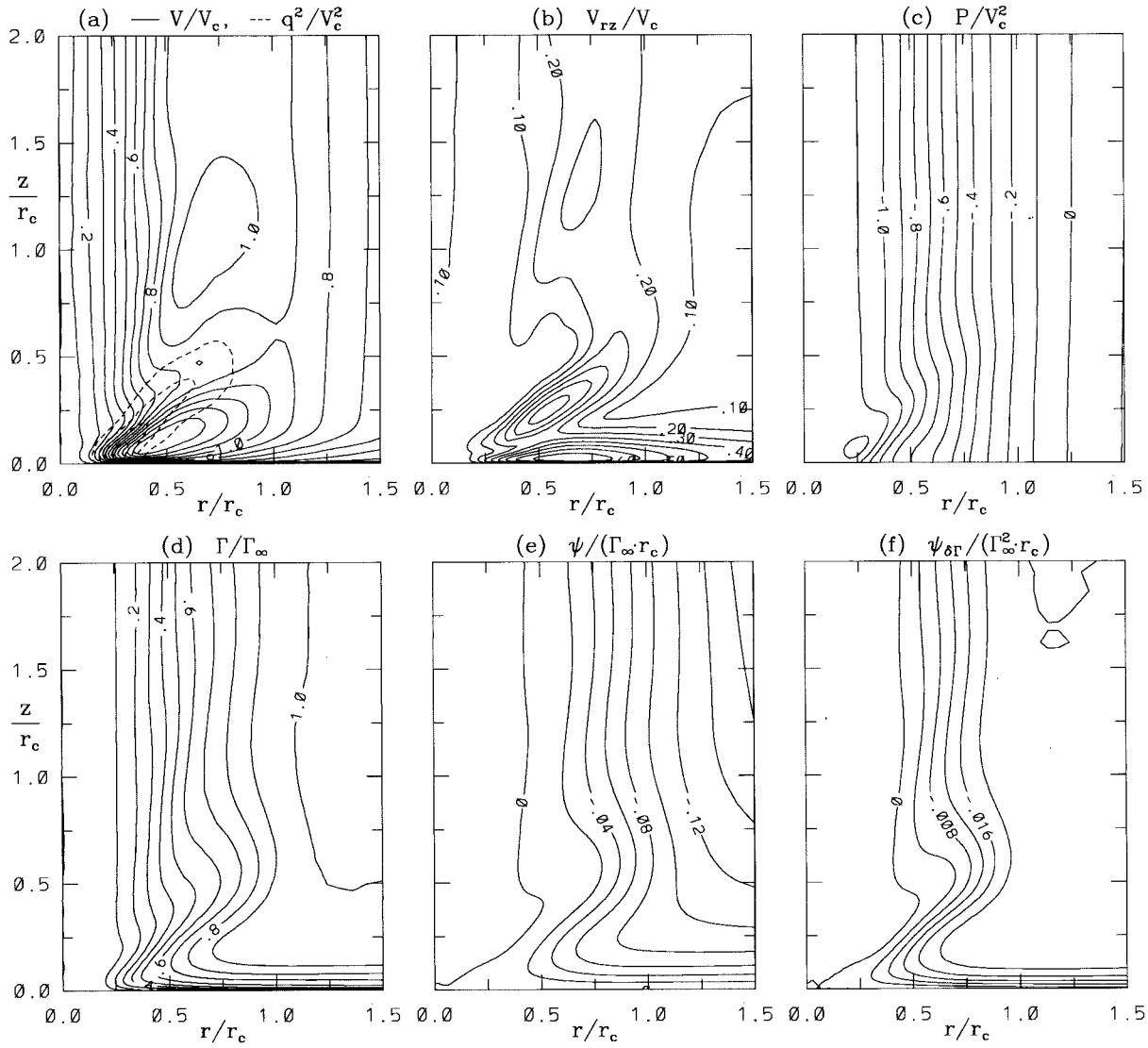

FIG. 1. Normalized, axisymmetric, time-averaged contours in the radial–vertical plane for the corner flow region of a sample high-swirl tornado vortex. (a) Swirl velocity (solid contours) together with highest levels of total velocity variance (dashed, contour level is 0.1), (b) magnitude of the velocity vector in the *r*–*z* plane, (c) perturbation pressure, (d) angular momentum, (e) streamfunction, (f) depleted angular momentum streamfunction.

well as the analysis of our numerical data, let us initially restrict the class of flows that we consider to ones with axisymmetric, time-independent outer boundary conditions. In these cases the mean flow can be obtained by taking a time average and is guaranteed to be axisymmetric about a known center line, even though the instantaneous flow is asymmetric, fully three-dimensional, and unsteady in time. When we discuss the effects of the translation of the tornado on the corner flow (among other variations considered in both sections 3 and 4 below) we will necessarily relax the axisymmetric requirement. The quasi-steady approximation is a good one in our study of the corner flow as long as the characteristic timescale of the corner flow itself is short compared to the timescales on which the larger-scale flow (which sets our boundary conditions) changes appreciably. The former timescale is typically of order 10 s (given corner flow length scales of tens to a few hundred meters and velocities of tens of meters per second), while the latter is of order a few minutes, so that this is, in general, a reasonable approximation. The flow conditions on the kilometer scale do change appreciably as a storm system evolves, however, so that a given tornado may be expected to display different corner flow structures over the course of its lifetime.

1) A HIGH-SWIRL CORNER FLOW

In Fig. 1 we have plotted normalized axisymmetric time averages of several flow variables from one of our

simulations to illustrate some of the general features of a tornado vortex corner flow. The figures show a radial–vertical cross section of the flow about the corner flow region of interest. This represents a small portion of the domain in which the simulation was actually performed; in particular, the inflow and outflow boundary conditions were initially set far from the corner flow itself. In Figs. 1a–c are shown, respectively, contours of the swirl velocity (V), the magnitude of the velocity in the radial–vertical plane (V_{rz}), and the perturbation pressure (p) (i.e., the pressure minus the hydrostatic component). Figures 1d–f show, respectively, contours of the angular momentum of the flow about the center line (Γ), the streamfunction (ψ) indicating the direction and integrated volume flux of the flow, and a depleted angular momentum streamfunction ($\psi_{\delta\Gamma}$) indicating the direction and integrated flux of the flow of fluid with low angular momentum. The latter will be defined precisely in section 2b below when we discuss quantitative measures of the corner flow. The tornado vortex structure is often discussed in terms of four distinct regions of the flow, which are readily identified in Fig. 1d: an outer region in which Γ is constant (or slowly varying) with value Γ_∞, a surface layer with sharp vertical Γ gradients and nearly zero vertical velocity, an upper-core region with strong radial Γ gradients and nearly zero radial velocity, and the corner flow region proper where the flow transitions from horizontal to vertical and all velocity components are significant. In the outer- and upper-core regions the flow is in approximate cyclostrophic balance and, consequently, is approximately cylindrically symmetric: any appreciable vertical gradients in the swirl field would give rise to vertical pressure gradients driving a vertical flow that would tend to eliminate the deviation from cylindrical symmetry. We have adopted the maximum swirl velocity in this upper-core region, V_c, as a characteristic velocity scale and $r_c \equiv \Gamma_\infty/V_c$ as a characteristic length scale for the purpose of presenting Fig. 1 (and subsequent plots) in nondimensional form. As an example of reasonable physical values for this case, we could take $V_c = 75$ m s^{-1}, and $\Gamma_\infty = 15\,000$ m^2 s^{-1}, giving $r_c = 200$ m and a core pressure drop of approximately 70 mb.

In the surface layer the pressure is to a good approximation equal to that set by the cyclostrophic balance in the cylindrically symmetric region above, since the vertical pressure gradient tends to be small near the surface. The swirl velocity, however, necessarily drops to zero at the surface due to surface friction, so that the flow in the surface layer is out of cyclostrophic balance. The radial pressure gradient, now exceeding the centripetal acceleration needed to turn the swirling flow, drives the radial velocity acceleration apparent in Fig. 1b. In the corner flow this radial surface jet, converging toward $r = 0$, is forced to turn into an (in this case) annular vertical jet (Fig. 1b), but not before overshooting the radial point at which the lowered Γ in the surface layer equals that in the cylindrically symmetric core region above (Fig. 1d). It is this inertial overshoot that leads to the highest swirl velocities generally being found near the surface within the corner flow (Fig. 1a), as well as the highest radial and vertical velocities (Fig. 1b) and lowest pressure drop (Fig. 1c). In Fig. 1a we have also indicated the region of largest turbulent kinetic energy, which coincides with the region of sharpest velocity gradients, again within the corner flow.

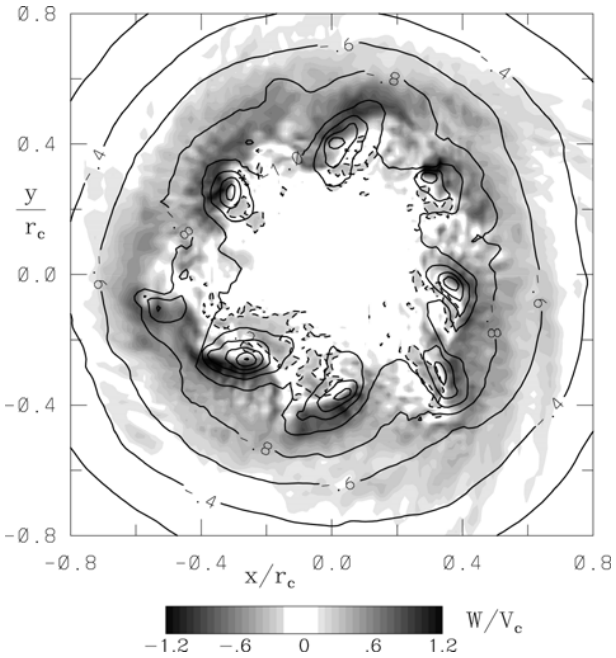

FIG. 2. Instantaneous horizontal cross section of simulated tornado from Fig. 1 at a height of 0.2 r_c, showing perturbation pressure (solid contours in units of ρV_c^2) and normalized vertical velocity (grayscale). The dashed contour indicates a normalized vertical velocity level of -0.2.

As can be seen in Figs. 1d–f, the Γ contours, mass flux streamlines, and depleted Γ streamlines are all nearly parallel with each other, showing that advection by the mean flow is the dominant transport mechanism for both the mass and angular momentum fluxes. A more careful inspection within the corner flow region itself shows that the contours are not exactly parallel here: there is significant turbulent angular momentum transport due to the secondary vortices as described in LLS97. Figure 2 shows the instantaneous pressure and vertical velocity contours on a horizontal slice through the corner flow at a height of $0.2r_c$, within the region of large turbulent kinetic energy (TKE) indicated in Fig. 1a. At this particular sample time, seven secondary vortices rotating about the main vortex are clearly evident. The strong up–down vertical velocity couplet associated with each secondary vortex is largely due to its tilt. As discussed in LLS97, the secondary vortices provide a net angular momentum transport directed radially inward into the central recirculating flow.

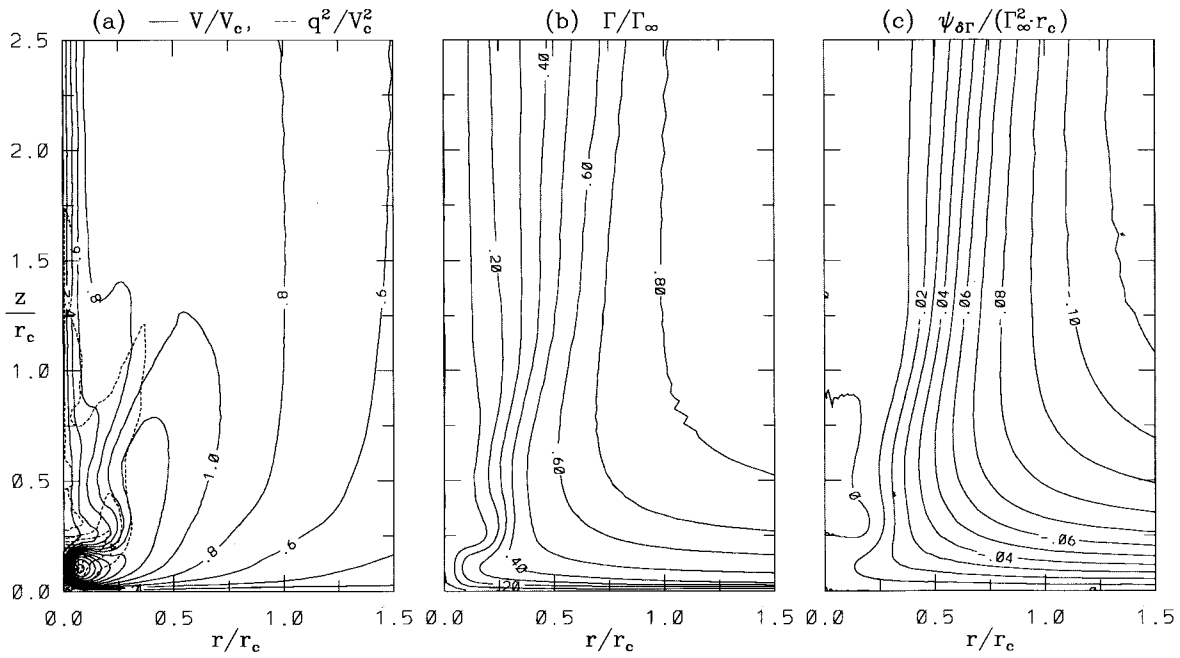

FIG. 3. Normalized, axisymmetric, time-averaged contours in the radial–vertical plane for the corner flow region of a sample low-swirl tornado vortex. (a) Swirl velocity (solid contours) together with highest levels of total velocity variance (dashed, contour level is 0.2), (b) angular momentum, (c) depleted angular momentum streamfunction.

2) A LOW-SWIRL CORNER FLOW

The vortex of Fig. 1 illustrates what is considered a ''high-swirl'' corner flow behavior. Figures 3 and 4, in contrast, show normalized time-averaged axisymmetric contours exhibiting a ''low-swirl'' corner flow. Figure 3a–c show contours of nondimensionalized swirl velocity, angular momentum, and depleted angular momentum streamfunction. In this case the most extreme velocities in the corner flow are pushed much closer to $r = 0$ (relative to r_c) than in the high-swirl example. In order to better illustrate what is happening in this case we zoom in to the scale of the inner corner flow in Fig. 4, showing the swirl velocity, velocity magnitude in the r–z plane, and perturbation pressure. The radial velocity in this case converges all the way to the axis to form an intense central vertical jet driven upward by an intense low pressure minimum above the surface. At the top of this surface jet is an abrupt vortex breakdown where the vortex core diameter increases dramatically. The radius where the peak swirl velocity occurs is more than a factor of 4 larger above the breakdown than it is below. The instantaneous view of this breakdown given in Fig. 5 shows that the turbulence in this low-swirl case is quite different from that in the high-swirl case of Fig. 2. For this case the resolved turbulence is primarily confined within and downstream of the breakdown. The broader region of large TKE in Fig. 4a is primarily a manifestation of the unsteadiness in the height of the breakdown and some wobble in the very narrow core jet upstream of the breakdown. The qualitative features distinguishing these high- and low-swirl cases in Figs. 4 and 1 are similar to those exhibited previously in laboratory flows (e.g., Church et al. 1979) and axisymmetric simulations (e.g., Lewellen and Sheng 1980). The primary difference here is the ability to also exhibit the character of the turbulence, which, particularly in the high-swirl case, will strongly affect the potential damage on the surface.

3) A VERY LOW SWIRL CORNER FLOW

In addition to high-, low-, and medium-swirl corner flows (such as illustrated above and in LLS97, respectively), studies of corner flows in tornado vortex chambers also identify a very low swirl regime. As the swirl ratio is dropped starting from a low-swirl vortex, the vortex breakdown is observed to occur progressively higher above the surface and its magnitude to progressively weaken [see, e.g., the review of Davies-Jones (1986)]. We exhibit axisymmetric time-averaged contours from a simulation with such a very low swirl corner flow behavior in Fig. 6. There is now no increase in the tangential velocity near the surface because the radial inflow separates from the surface well outside of the upper-core radius. The negative radial pressure gradient induced by the decelerating radial inflow in the surface layer is now large enough to overcome the swirl-induced positive pressure gradient even outside of the upper-core radius (cf. the nearly flat pressure contours near the surface in Fig. 6c). The resulting slight adverse

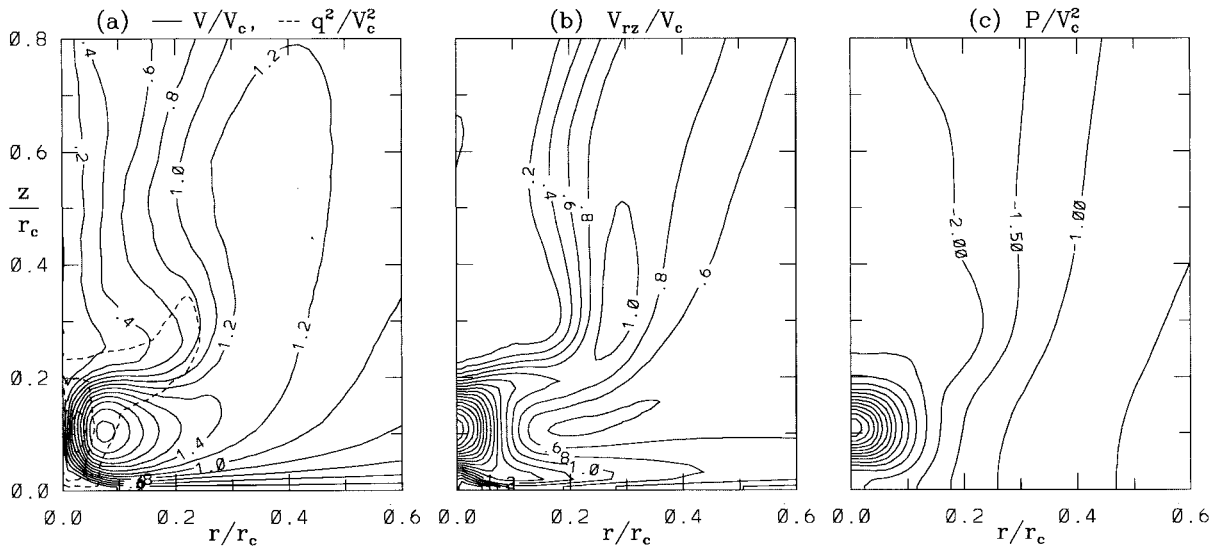

FIG. 4. The inner corner flow for the low-swirl vortex of Fig. 3. (a) Swirl velocity (solid contours) together with highest levels of total velocity variance (dashed, contour level is 0.5), (b) magnitude of the velocity vector in the *r*–*z* plane, (c) perturbation pressure.

pressure gradient is sufficient to force the surface layer flow to separate from the surface outside of r_c as seen in Fig. 6b. This effectively prevents any vortex intensification near the surface. What weak intensification that does occur is located approximately a core radius or more above the surface. About the only signatures for this intensification remaining in Fig. 6 are the weak central pressure minimum toward the top of the figure and an almost imperceptible increase in core size and drop in peak swirl velocity above this level.

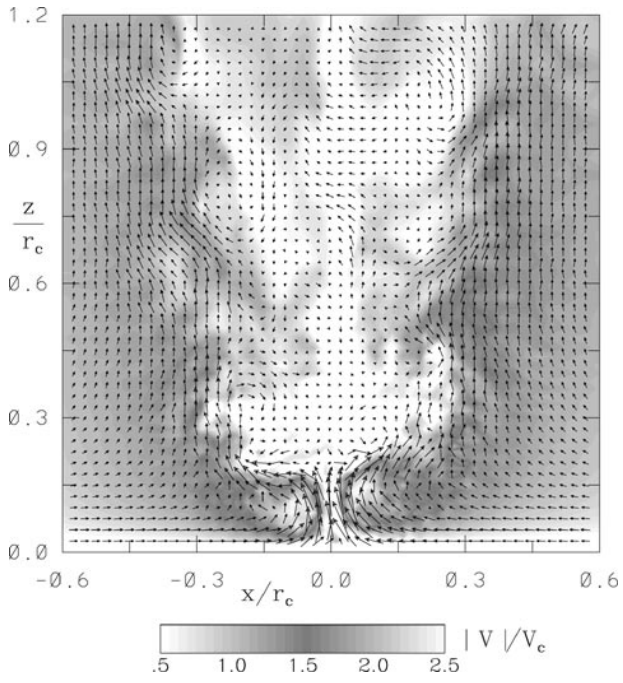

FIG. 5. Instantaneous vertical cross section of simulated tornado from Fig. 4 showing normalized absolute swirl velocity (grayscale) and magnitude of the velocity vector in the *r*–*z* plane (arrows, interpolated onto a uniform grid for clarity; maximum length corresponds to $V_{rz}/V_c = 3.8$).

While this example fits the picture of a very low swirl corner flow coming from the laboratory studies, we have achieved it here in quite different fashion than is usually encountered in tornado vortex chambers. We could have taken the conditions of the low-swirl example in Fig. 3 and reduced the swirl ratio of the larger-scale flow by either increasing the overall horizontal convergence, a_c, or decreasing the incoming Γ level, in order to achieve this corner flow behavior. Instead, the simulation of Fig. 6 has the same domain size and imposed Γ and a_c on the inflow boundaries away from the surface as the high-swirl example of Fig. 1; that is, the outer tornado-scale flow would be characterized as having high swirl. The very low swirl corner flow evidenced in Fig. 6 was achieved by including a layer of zero swirl fluid near the surface in the outer inflow boundary conditions. In our previous two examples, frictional losses to the surface from the base of the large-scale vortex produced the low angular momentum fluid in the surface layer. This is not the only possible source of low-swirl fluid, however. The low-swirl fluid in the surface layer can be transported over relatively large distances, with its possible origins including preexisting low angular momentum fluid either initially outside of or below the outer-scale tornado vortex. Such conditions might arise, for example, from any evolutionary process for the mesocyclone that does not create a uniformly swirling flow all the way to the surface. As the example of Fig. 6 illustrates, changes in the flow within tens of meters of the surface can dramatically affect the intensity and structure of the corner flow even if those changes are

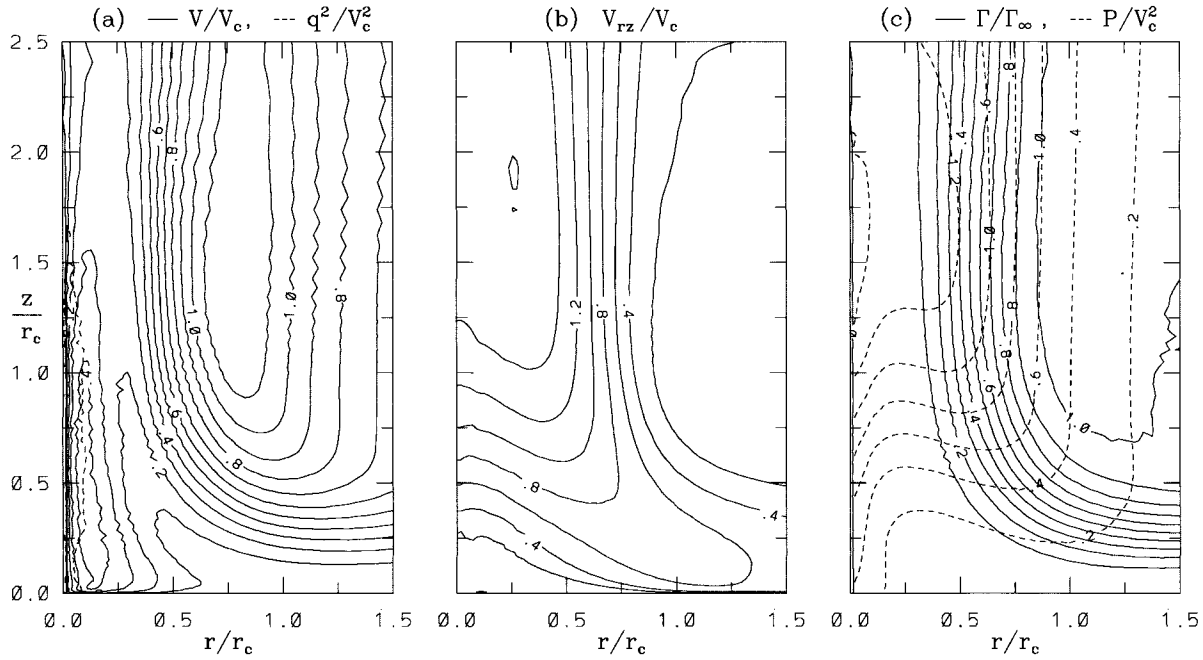

FIG. 6. Normalized, axisymmetric, time-averaged contours in the radial–vertical plane for a very low swirl vortex. (a) Swirl velocity (solid contours) together with highest levels of total velocity variance (dashed, contour level is 0.2), (b) magnitude of the velocity vector in the r–z plane, (c) perturbation pressure (dashed) and angular momentum (solid).

imposed many hundreds of meters away from the vortex center.

If, as is sometimes argued, we consider the core flow to be an extension of the surface layer and vortex breakdown to be somewhat analogous to a boundary layer separation (cf. Hall 1972), then the corner flows in Figs. 1, 3, and 6 differ by where the separation of the strong surface layer–core flow occurs relative to the upper-core radius. This flow separates from the surface at a radius that is a sizable fraction of r_c for ''high swirl'' (Fig. 1), at smaller radius for medium swirl, after turning the corner to form the central core flow for ''low swirl'' (Fig. 3), and finally well above the surface for ''very low swirl'' (Fig. 6). It is this sort of continuous change in structure that we would hope to quantitatively parameterize with an appropriately defined corner flow swirl ratio, independent of whether that change was achieved through changing the large-scale swirl conditions, low-level inflow conditions, surface roughness, upper-core structure, etc.

b. Defining a local corner flow swirl ratio

We consider the three most important dimensional parameters affecting the corner flow to be a characteristic angular momentum, mass flux, and upper-core size for the surface layer–core flow, denoted Γ^*, $\mathcal{M}^*$, and r^*, respectively. From these we can form a dimensionless swirl ratio,

$$S_c \equiv \Gamma^* r^* / \mathcal{M}^*. \tag{1}$$

Obviously there is some arbitrariness in defining Γ^*, $\mathcal{M}^*$, and r^*. For our purposes we would like definitions that can be easily and robustly computed from our simulations; other choices might prove more convenient or accessible for laboratory or field measurements. By ''robust'' we mean that the values measured for these quantities, which should all be measurable outside of the corner flow region itself, should not be overly sensitive to the particular choice of radius or height at which they are measured. We take Γ^* to scale with Γ_∞, the angular momentum level immediately outside of the surface and core regions. For r^* we use r_c as we defined it above for nondimensionalizing our figures. This choice agrees with the definition of core radius often used for some idealized core profiles such as the Rankine vortex but is by no means unique. Different measures of the core radius are distinct to the extent that the shapes of the Γ profiles across the core differ, a level of detail that can be important (as we will illustrate in section 4) but that is impossible to incorporate into a single parameter. Figure 7 shows profiles of Γ/Γ_∞ and V/V_c in the upper core versus r/r_c from a representative sample of our simulations to illustrate the range of variation encountered. It illustrates as well why we have not chosen to use the radius at which the swirl velocity is a maximum for our definition of core radius, as is often done. In each case shown there exists a broad range of radii over which V is within 80% of V_c; modest changes in the Γ profile can then shift the location of the absolute peak by more than a factor of 2 in radius.

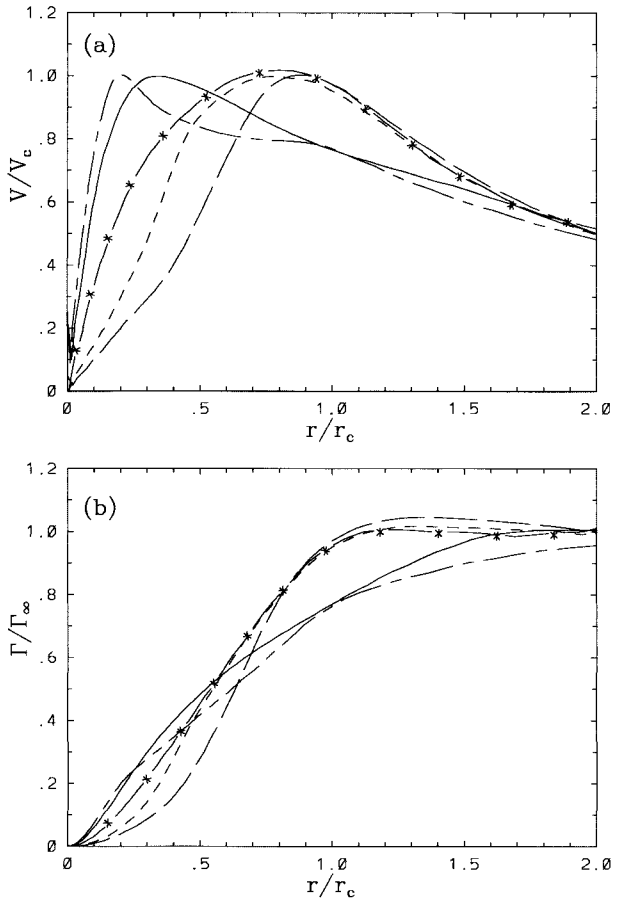

FIG. 7. Axisymmetric, time-averaged radial profiles in the quasi-cylindrically symmetric upper cores of five sample simulated tornado vortices. (a) Normalized swirl velocity V/V_c, (b) normalized angular momentum Γ/Γ_∞.

The swirl velocity profile sometimes even has more than one local maximum.

In choosing $\mathcal{M}^*$ we must distinguish between mass flow associated with the surface layer and core versus that in the outer converging swirling flow. Ideally the definition of $\mathcal{M}^*$ should also be based only on conserved or nearly conserved quantities, so that the flux can be measured at some radius before entering, or at some height after exiting, the corner flow region with the result being relatively insensitive to the precise radial or vertical position chosen.

Away from the boundaries both the mean mass flux and the mean angular momentum flux through any region are conserved in a flow that is steady and axisymmetric in the mean. We take the density to be constant within our domain of interest. In the region just outside of the surface and core flows, Γ is nearly constant as well, so that in this region the fluxes are carried together in simple fashion. This is not the case within the surface-corner-core flow; a distinguishing feature of this region is that Γ is necessarily strongly varying. An appropriate combination of the two fluxes, the flux of $\Gamma_d \equiv \Gamma_\infty - \Gamma$ (''depleted angular momentum''), is then to a good approximation nonvanishing within our domain only within the surface–corner–core flow, thus providing a useful conserved signature for these regions. The conservation equation,

$$\nabla \cdot \langle \mathbf{V}\Gamma_d \rangle = \frac{\partial \langle w\Gamma_d \rangle}{\partial z} + \frac{1}{r}\frac{\partial}{\partial r}(r\langle u\Gamma_d \rangle) = 0, \qquad (2)$$

can be derived from the azimuthal momentum and continuity equations. Here w and u are the axial and radial velocity components, and the angular brackets denote both a time and an axisymmetric average. The bracketed terms include both the mean and turbulent fluxes of depleted angular momentum. The Reynolds number is assumed sufficiently large that laminar viscous stress terms may be neglected. Note that $\langle w\Gamma_d \rangle$ is not equal to zero at the surface but, rather, equal to a subgrid turbulent flux transported to the surface, which is parameterized in terms of an effective surface roughness, z_0, in our model. Given (2) we can define a depleted angular momentum streamfunction in analogy with the usual streamfunction for a turbulent flow that is steady and axisymmetric in the mean, such that

$$\langle w\Gamma_d \rangle = \frac{1}{r}\frac{\partial \psi_{\delta\Gamma}}{\partial r}, \qquad \langle u\Gamma_d \rangle = -\frac{1}{r}\frac{\partial \psi_{\delta\Gamma}}{\partial z}, \qquad (3)$$

with

$$\psi_{\delta\Gamma}(r, z) - \psi_{\delta\Gamma}(r_0, z_0) = \int r'(\langle w\Gamma_d \rangle\, dr' - \langle u\Gamma_d \rangle\, dz'). \qquad (4)$$

The line integral in (4) can be taken along any curve in the axial plane joining the point at (r, z) with the reference point at (r_0, z_0). In plotting $\psi_{\delta\Gamma}$ in Figs. 1f and 3c the reference point was chosen on the axis so that $\psi_{\delta\Gamma}(r_0, z_0) = 0$. In the figures the depleted Γ flux streamlines are concentrated within the surface–corner–core flow regions, as advertised; were a larger radial domain shown, one could see some of the streamlines eminating from the surface, representing the loss of angular momentum there. In general, there are two primary ''sources'' of depleted Γ flux: the frictional loss of angular momentum from the outer swirling flow to the surface, and low Γ fluid from large radius outside or initially below the outer swirling flow. In addition, low Γ fluid from above can be drawn down the vortex core, and angular momentum can be turbulently transported radially out of the upper core, increasing the depleted Γ flux in the upper core.

We now define Υ to be the total depleted Γ flux flowing through the corner flow region. Because there is very little angular momentum lost to the wall within the corner region itself (relative to the total), the flux into the corner equals the flux out of the corner to a good approximation; that is,

$$\Upsilon \approx 2\pi \int_0^{z_1} -\langle u(r_1, z)\Gamma_d(r_1, z)\rangle r_1 \, dz$$

$$\approx 2\pi \int_0^{r_2} \langle w(r, z_2)\Gamma_d(r, z_2)\rangle r \, dr, \qquad (5)$$

where r_1 is a radius close to, but outside of, the corner flow, z_1 is a height safely above the surface layer, z_2 is a height just above the corner flow, and r_2 is a radius safely outside of the upper-core region. Thus $\Upsilon = 2\pi\psi_{\delta\Gamma}$ evaluated immediately outside of the corner flow region. In our simulations, we have confirmed the equality of the last two terms in (5) and their insensitivity to the precise choices of r_1, z_1, r_2, and z_2, generally to a level of a few percent. Note that Υ can be computed even when the time-averaged flow is not exactly axisymmetric, and, in fact, Eqs. (2)–(4) remain valid in this case.[2]

We can now define an $\mathcal{M}^*$ meeting our requirements if we take it to scale with Υ/Γ_∞. The specific form of the local corner flow swirl ratio (1) that we will use to analyze our simulations is then

$$S_c = r_c\Gamma_\infty^2/\Upsilon. \qquad (6)$$

Other possible implementations of (1) may differ from this one in practice to the extent that changes in the shape of the Γ and flux profiles in the core and surface layer are important, a level of secondary detail that we do not attempt to capture with a single parameter. For the high-swirl vortex of Fig. 1, $S_c = 6.9$; for the low-swirl case of Fig. 3, $S_c = 1.2$; and for the very low swirl case of Fig. 6, $S_c = 0.75$. We attribute the change in corner flow behavior in the three cases primarily to the change in depleted Γ flux in the surface layer (cf. Figs. 1f and 3c). For reference, the nontranslating medium-swirl simulation presented in LLS97 has $S_c = 2.6$.

c. Dependence of S_c on selected physical parameters

The S_c in (6) can be interpreted as the ratio of a characteristic swirl velocity in the surface–core flow ($\Gamma_\infty/r_c = V_c$) to a characteristic flow-through velocity ($\Upsilon/\Gamma_\infty r_c^2$), justifying its consideration as a swirl ratio. Unlike the swirl ratios commonly used in laboratory studies of vortex breakdown in vortex tubes or of vortex structure in tornado vortex chambers, however, it is by construction specific to the surface–core flow and does not explicitly involve the larger-scale geometry, for example, the radius of the vortex chamber. This is useful since the analog of the latter scale is not easily identified in an actual thunderstorm system. On the other hand, while the ingredients of (6) can be measured, r_c and Υ, in particular, cannot easily be set directly in any laboratory or numerical experiment. Nor are they completely independent of each other: the impact on S_c of an increase in Υ is generally partly offset by the increase in r_c associated with carrying the increased depleted Γ flux up the core.

In section 3 we will examine to what extent the dependence of the corner flow on the velocity fields immediately outside of the corner flow is parameterized by S_c alone. Here we examine first, at least qualitatively, how S_c varies with some selected physical parameters affecting the larger-scale boundary conditions, assuming that each parameter is varied in isolation. First consider the dependence on the swirl ratio of the larger-scale converging swirling plume in which the core flow is embedded. We can define this, following LLS97, as

$$S_{\text{outer}} = \Gamma_\infty/(a_c r_0 h_{\text{inf}}), \qquad (7)$$

where the inflow layer has a height h_{inf}, begins at a radius r_0, has angular momentum Γ_∞, and average horizontal convergence a_c. Increasing r_0 allows the flow more opportunity to lose angular momentum to the surface, thereby increasing Υ and decreasing S_c. Increasing either a_c or h_{inf} will generally decrease the upper-core radius, again reducing S_c. With other conditions fixed, S_c rises or falls with S_{outer}, as one would expect.

On the other hand it is possible to vary S_c over a large swirl range with S_{outer} held fixed. For example, it has been noted by many studies that an increase in surface roughness leads to a ''lower-swirl'' corner flow behavior (e.g., Leslie 1977). This trend is incorporated into S_c, which provides a quantitative measure for it: as the surface roughness is increased, the angular momentum loss to the surface is increased, with a corresponding increase in Υ and drop in S_c. Any source of low angular momentum fluid into the boundary layer flow at large radius also serves to reduce S_c by increasing Υ (as seen, e.g., in the case of Fig. 6). Adding a translation velocity to the vortex can have this same effect; we consider such an example in section 4b.

In general, anything that increases the upper-core radius without affecting the surface layer flow outside of the corner flow region will increase S_c. Examples include decreasing the ratio of the inflow height to the domain height where the upper boundary conditions are imposed, adding an upper-level central downdraft, the addition of horizontal divergence in the upper flow, or the imposition of nonswirling flow through the lateral boundaries above some height.

We could, of course, include an arbitrary multiplicative constant in the definition of S_c in (6) but have chosen not to do so. The domain swirl ratio used in laboratory investigations of corner flow (e.g., Church et al. 1979) tends to have smaller values than S_c for

[2] The conservation of angular momentum is a consequence of the underlying rotational invariance of the Navier–Stokes equations themselves and requires no further assumptions about the symmetry of a particular flow solution. The simple form of Eq. (2) arises from the assumption of a steady mean flow, high Reynolds number, and the fact that torques exerted by pressure gradients and transport by the swirl velocity component both cancel out after performing an azimuthal integration.

similar corner flow behavior, but there is not a one-to-one correspondence between the two quantities in general. They measure different properties of the flow, and S_c is affected by other factors in addition to the domain swirl ratio.

3. Summary of dynamical relationships in the corner flow

In general, varying any physical parameter in the tornado flow will affect not only S_c, but the structure of the velocity profiles in the surface layer and upper core as well. In this section, we explore to what extent the effect on the corner flow of any such change is captured solely through its effect on S_c. In the limited space available in this paper it is not possible to show velocity distributions from all of the simulations performed for this study. Instead, we present here some dimensionless ratios of vortex flow parameters for a relatively large, representative set of simulations. In this dataset we tried to cover a range of different, but realistic, flow conditions occurring immediately outside of the corner flow region. We did not attempt to impose boundary conditions there directly, however. Instead, this was achieved indirectly by varying our far-field boundary conditions well outside of the corner flow region. In essence we used a large part of our simulation domain to provide more realistic turbulent boundary conditions for the corner flow, starting from more idealized steady flow conditions imposed on the outer tornado scale. The range of idealized conditions chosen was intended only as rough approximations to some of the wide variety of conditions expected to exist in real tornadoes on this larger-scale domain. In general, we imposed a region of inflow on the outside lateral boundaries of our simulation with a constant Γ and constant horizontal convergence, a_c. We varied the ratio of the inflow height to the full domain height, as well as the domain size, Γ and a_c. The boundary condition at our domain top was taken as zero slope on v and u with either a uniform outflow velocity across the full domain, or through a disk of fixed size, sometimes including an imposed central downflow (with no swirl) in a disk of given radius. In many of our runs the imposed constant Γ and a_c inflow region extended to the ground, so that the surface layer of depleted Γ flow developed on its own due to surface friction as the flow proceeded radially inward. In others, we imposed an analytic boundary condition on the surface flow, as described in LLS97, and in still others we included a layer of imposed inflow over the surface of fixed height with no swirl at all. The dataset includes an order of magnitude variation in the effective surface roughness and some simulations with a realistic translation velocity. In addition, we have included a simulation with horizontally diverging flow imposed in the upper half of the domain, and another in which the imposed lateral inflow has zero swirl over the top three-quarters of the domain. Obviously we have not independently covered the full parameter space in any of these variations; nonetheless, the dataset is large and we can only summarize some results in this work. It is our intent to present some of our more specialized results from this dataset in future work.

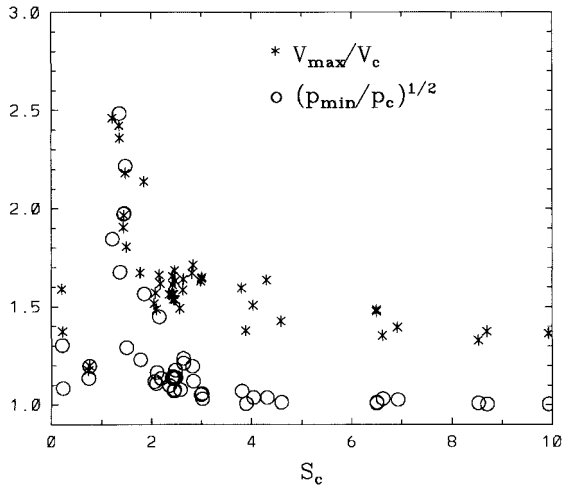

FIG. 8. Summary of the surface intensification of the vortex for a set of 50 simulations as measured by the ratios V_{max}/V_c (*) and $\sqrt{p_{min}/p_c}$ (○) vs S_c.

Each simulation was performed, and the data analyzed, as described in LLS97. We ran each simulation until quasi-steady conditions were achieved, so that the initial conditions were not critical, and continued to run for long enough to collect a good statistical sample for time averages. We employed a stretched grid spacing in all three dimensions so that we could achieve a fine grid spacing within the corner flow region of immediate interest while still taking our domain boundaries (where we set the inflow and outflow conditions described above) far from the corner flow. For computational efficiency we allowed the flow to spin up on a series of grids, progressing from coarse to fine. In each case, we refined the grid enough so that the average statistics (as well as the qualitative instantaneous flow structures) agreed for the finest and next-to-finest grid simulations. In some cases the finer grid simulations were performed in a smaller computational domain (but still much larger than the corner flow region) with boundary conditions inherited from the coarser simulation. The results presented here are only from the better resolved of our simulations, though the next-best-resolved cases gave results entirely consistent with these. Unless otherwise noted, the averages referred to involve both an axisymmetric and a time average in order to improve the statistics.

In Fig. 8 we show two variables as a function of swirl that provide measures of the surface intensification of the tornado relative to the core flow above. One is the ratio of the maximum average swirl velocity, V_{max}, to the maximum average swirl velocity in the quasi-cylinderical region above the surface boundary layer, V_c. The

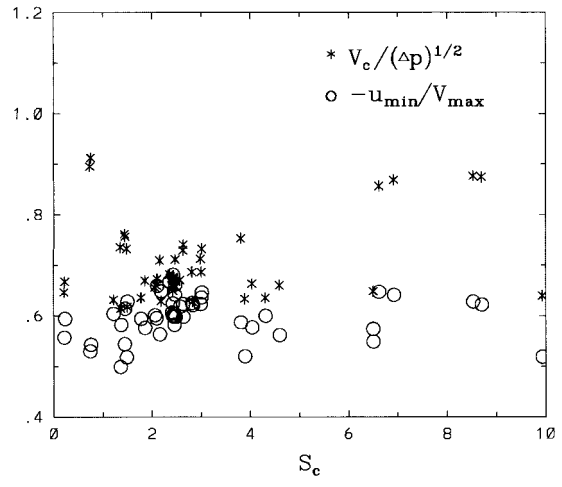

FIG. 9. Summary of the two ratios $V_c/\sqrt{\Delta p}$ (*) and $-U_{\min}/V_{\max}$ (○) vs S_c from sample simulations.

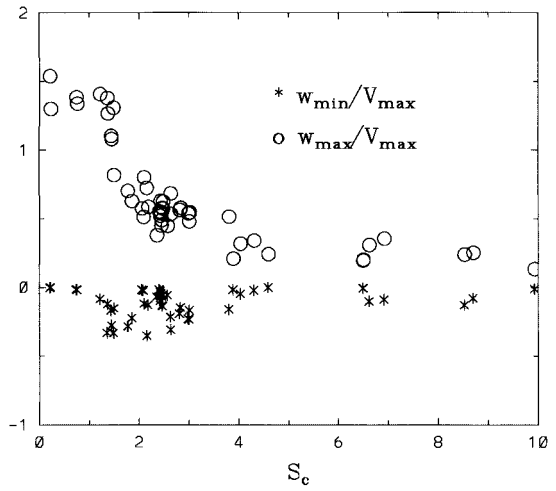

FIG. 10. Summary plot of the ratios $W_{\min}/V_{\max}$ (*) and $W_{\max}/V_{\max}$ (○) vs S_c from sample simulations.

other is the ratio of the minimum average pressure, $p_{\min}$, to that in the quasi-cylinderical region above the surface boundary layer, p_c. We show the square root of the pressure ratio to make it more similar to the velocity ratio. There is noticeable scatter, but both ratios show a distinct peaking of the intensification for S_c around 1.2. The peak intensification occurs for low-swirl corner flows such as in Fig. 4, where a sharp vortex breakdown caps a strong central jet just above the surface. For increasing values of S_c, the core size near the surface progressively increases to approach that of the core above as the radial overshoot in the surface layer weakens. For decreasing values of S_c below about 1, the vortex breakdown occurs at greater heights with decreasing changes across it, eventually weakening sufficiently that the term ''breakdown'' is no longer appropriate. A similar behavior has been observed in laboratory observations (e.g., Snow 1982). The most interesting feature of Fig. 8 is the sharpness of the intensification peak, though there is some inherent uncertainty in both its width and position due to the breadth of variations in boundary conditions we employed in order to vary S_c. Less scatter in the curve would be expected if we were to cover the swirl range by varying only a single physical parameter such as the outer-scale swirl ratio, or the surface roughness. The apparent gaps in the values of S_c represented are purely a selection effect: in generating a range of S_c values indirectly by varying different physical parameters we have not evenly populated the space.

Figure 9 shows the ratio of V_c to the square root of the pressure drop between the inflow and the center of the quasi-cylindrical region, and the ratio of the minimum average radial velocity, $U_{\min}$, to $V_{\max}$. Both of these ratios are remarkably insensitive to the swirl ratio. They show some scatter across the range of variations, but not as much as might be expected considering the range of flow profiles in the plots exhibited in sections 2 and 4. The values of $V_c/\sqrt{\Delta p}$ are scattered about a central value of 0.7, a little above the value of 0.6 associated with the cyclostrophic pressure drop of a Burger–Rott swirl velocity profile (Rott 1958). The near constancy of the ratio $U_{\min}/V_{\max}$ (with value ≈ -0.6) is a reflection of the direct dependence of the swirl overshoot on the overshooting low-level radial inflow. The degree of constancy is, however, surprising. The peak inflow occurs quite close to the surface a little outside the radius of the maximum swirl velocity; in general, the two peaks lie on different streamlines.

The velocity components in the corner flow do not all scale the same way with swirl ratio as Fig. 9 might suggest. Figure 10 shows the ratio of the maximum and minimum average vertical velocities to the maximum average swirl velocity. Not surprisingly, $W_{\max}/V_{\max}$ decreases with increasing swirl. It is not clear how significant the near constancy of this ratio is for $S_c < 1$. It is consistent with what is known about vortex breakdown that all of the low-swirl cases where a breakdown is observed have $W_{\max} > V_{\max}$. The values $W_{\max}/V_{\max} \approx 1.4$ and $V_{\max}/V_c \approx 2.5$ for the low-swirl case are not far from the values of 2 and 1.7 deduced in the model of Fiedler and Rotunno (1986) and the corresponding values of 1.6 and 1.7 from the axisymmetric simulations of Fiedler (1993). The maximum downward velocity in Fig. 10 occurs on the high-swirl side of the peak intensification in Fig. 8 where the bowl or conical nature of the dividing streamline between the high-swirl flow and the recirculating flow is more gradual than the very abrupt divergence in the breakdown shown in Figs. 3–5.

Figures 8–10 demonstrate that much of the influence of the outer-scale variables studied here is captured by our low-level swirl ratio. Figure 11, giving some information on the fluctuations within the flow, suggests that this is not the complete story. Rather than show the rms values of the fluctuations, we show the average of the peak fluctuations at any time: mean peak negative

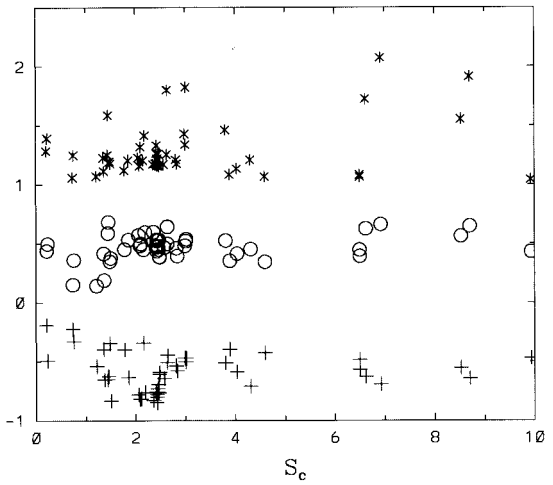

FIG. 11. Measures of the turbulent intensity as given by the average of instantaneous peak quantities from sample simulations: $p_{\min}^{\text{inst}}/p_{\min}$ (*), $(W_{\max}^{\text{inst}} - W_{\max})/V_{\max}$ (○), $(W_{\min}^{\text{inst}} - W_{\min})/V_{\max}$ (+).

pressure normalized by $p_{\min}$, mean peak positive vertical velocity minus $W_{\max}$ normalized by $V_{\max}$, and mean peak negative vertical velocity minus $W_{\min}$ normalized by $V_{\max}$. None of these combinations shows a clear trend with S_c. They do show that the peak instantaneous values can have significantly greater magnitudes than the mean values, and that the scatter in these values for a given value of S_c is greater than it is for the average variables, a topic we turn to in the next section.

4. Some tornado vortex features not characterized by swirl ratio alone

The behavior of the tornadic corner flow is, of course, governed by the velocity and pressure fields immediately outside of the corner flow region. A single quantity such as S_c, based on integral invariants of these fields, cannot, on its own, completely parameterize this dependence, although it seems to do a good job on the basic behavior of the mean flow. We expect, for example, that the distributions of the mass and angular momentum fluxes (and not just their integrated totals) should also have some effect on the corner flow behavior. We present here a sample of some of these effects.

a. Secondary vortex structure

Figure 12 shows the normalized swirl velocity, angular momentum, and depleted angular momentum streamfunction for a simulation with $S_c = 6.6$, that is, effectively the same value as for the simulation of Fig. 1. The two simulations were performed with the same Γ_∞ and achieve effectively the same depleted Γ flux in the surface layer and upper-core size as measured by r_c. The flows outside of the corner flow region differ chiefly in the angular momentum gradients in the upper-core region. In the case of Fig. 12 a weaker horizontal convergence was imposed on the side boundaries than for the case of Fig. 1, but a uniform vertical outflow was imposed on the top boundary instead of a weak central down-flow as for Fig. 1. The result is an upper core with nearly the same r_c, but with much sharper radial Γ gradients in the case with imposed down-flow and stronger convergence. The effect on the mean profiles in the corner region is largely to shift the location of the peak swirl velocity relative to r_c (with the vortex without a central downdraft having the peak at much smaller radius), but without significantly affecting the magnitude of the velocity overshoot (cf. Fig. 8). The effect on the instantaneous flow structure in the corner is more dramatic (as suggested by the pressure results in Fig. 11). Figures 2 and 13 show the instantaneous pressure and vertical velocity contours for the two cases on a horizontal slice through the corner flow. The former case, with the stronger Γ gradients, displays strong secondary vortices as noted earlier. The number of secondaries is not constant in time, and their evolution is often chaotic, but there are always a number of strong secondaries in this case, typically with perturbation pressure deficits of twice that in the upper core of the main vortex. In contrast, Fig. 13 is dominated by the central vortex supported by a lower pressure aloft (in units of V_c^2), with no strong secondary vortices in evidence at this (or other) times. A high-swirl corner flow is necessary to obtain multiple strong secondary vortices but clearly not sufficient. High S_c assures an eruption of flow from the surface layer at relatively large radius, which is a necessary ingredient for multiple secondary vortices, but does not guarantee strong radial gradients in the swirl or vertical velocities, which are also required to produce strong secondaries. Note that the local pressure intensification apparent in the secondary vortices of Fig. 2 is washed out upon taking an axisymmetric average and so does not appear in the measure used in Fig. 8.

b. Translation effects

Superposing a translation velocity (relative to the ground) with an imposed axisymmetric, converging, swirling outer tornado flow has the effect of breaking the mean axisymmetry within the surface layer flow. We perform our simulations in the frame of reference moving at constant velocity with the translating tornado vortex, so that the surface plane is prescribed to move in the opposite direction. The added surface shear stress due to the translation of the surface provides a torque that tends to enhance the angular momentum in the surface layer (defined about the center of the vortex well off the ground) on the side of the vortex where the swirl velocity and surface motion are aligned, and to reduce the angular momentum on the opposite side where they are opposed. This effect is purely due to the surface friction; in the limit of a smooth surface and inviscid

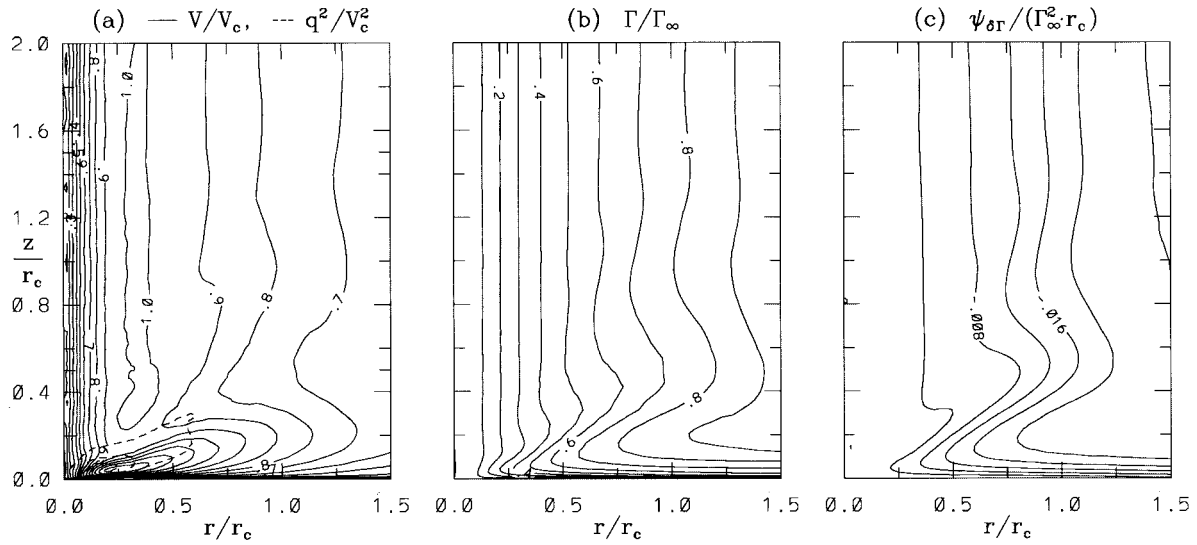

FIG. 12. Normalized, axisymmetric, time-averaged contours in the radial–vertical plane for a simulation with the same S_c as Fig. 1, but without the imposed central downdraft at the domain top and with a lower horizontal convergence. (a) Swirl velocity (solid contours) together with highest levels of total velocity variance (dashed, contour level is 0.1), (b) angular momentum, (c) depleted angular momentum streamfunction.

flow, the uniform translation would have no effect. The surface interaction is most important at larger radii where the relative magnitude of the translation velocity compared to the swirl velocity is greater, as is the lever arm for the torque and the area over which it acts. This asymmetry far from the vortex center is reduced as the flow spirals in close to the center; near the center the mean flow of a persistent vortex will always tend toward axisymmetry. This is partly achieved in trivial fashion by a shift in the vortex center near the ground as well as by the mixing of the different fluid populations. More importantly, at large radii where the flow is more asymmetric, it is the fluid with lower angular momentum that is preferentially drawn toward the vortex center. Consequently, the depleted Γ flux entering into the corner flow is enhanced over what it would be without the surface translation, driving the flow toward lower corner flow swirl ratio. For example, we have found that the addition of translation to a medium-swirl vortex can drive it to the low-swirl configuration characterized by dramatic low-level intensification and a strong surface jet below a (now asymmetric) vortex breakdown.

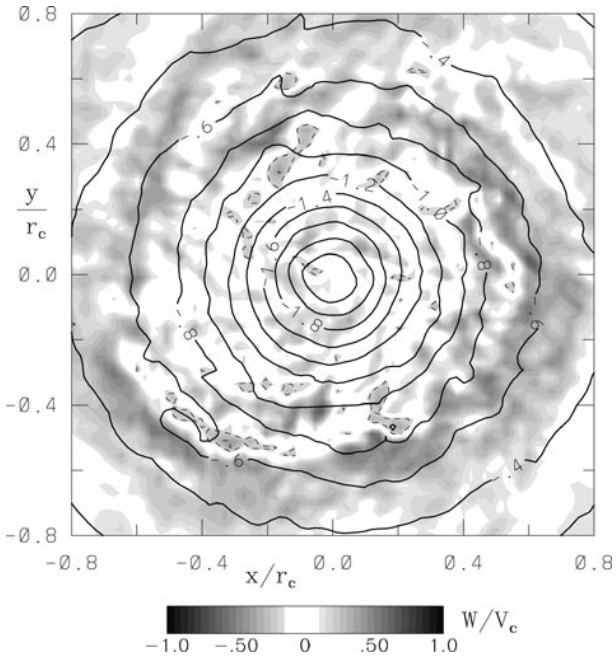

FIG. 13. Instantaneous horizontal cross section of simulated tornado from Fig. 12 at a height of 0.2 r_c, showing normalized perturbation pressure (contours) and vertical velocity (grayscale). The dashed contour indicates $W/V_c = -0.2$.

The shift of the mean vortex center near the surface by the translation complicates the quantitative application of the formulas of section 2. For simplicity, we consider the high swirl flow of Fig. 1, with an imposed translation velocity of 40% of V_c (cf. LLS97 for a comparison of a medium-swirl vortex with and without translation). In addition to implementing the translation into our surface boundary condition, we incorporated it into the lateral domain boundary conditions by superposing a logarithmic boundary layer aligned with the translation (with depth of 10% of the domain radius) onto the existing axisymmetric outer boundary condition. When, as in this case, the shift in the vortex center induced by the translation is small compared to the upper-core radius, we can safely ignore the shift to lowest order in analyzing the flow. In this particular case, as advertised, the addition of the translation has the effect

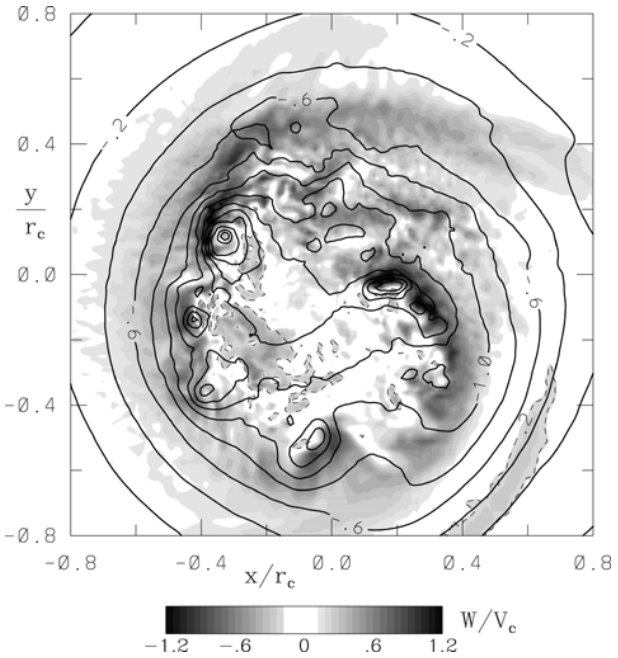

FIG. 14. Instantaneous horizontal cross section at a height of 0.2 r_c of a simulation like that of Fig. 2, but with the vortex translating relative to the ground to the right. Normalized perturbation pressure (contours) and vertical velocity (grayscale). The dashed contour indicates $W/V_c = -0.2$.

of lowering S_c, here from 6.9 to 4.9, due almost entirely to an increase in Υ. In addition, the translation adds an asymmetry and increased unsteadiness to the instantaneous flow structures in the corner flow. Figure 14 shows the pressure and *w* contours on a horizontal slice as in Fig. 2, but for the translating case. While the particular features change in time, the general character does not. In the translating case there are generally fewer secondary vortices lying closer to the center of the main vortex than in the nontranslating case, consistent with the modestly lower swirl ratio. The secondaries are no longer on equal footing with one another: typically one or two are considerably stronger than the rest. In addition, the preferential inflow of lower angular momentum fluid from one side of the large-scale vortex leads to the appearance of inwardly spiraling rolls in the surface layer (just apparent on the right-hand side of Fig. 14).

c. *More complex corner flows*

The magnitude of the local velocity overshoot in the corner flow is a function of (among other things) the local Γ and radial mass flow. Equation (6) relates S_c to certain averages of these quantities without any detailed knowledge of how the mass flow is distributed among different Γ levels, although this could clearly influence the structure of the corner flow. In particular, this affects the Γ value giving the peak overshooting swirl velocity and allows nested corner flow behaviors on different radial scales as demonstrated by our next example. Fig-

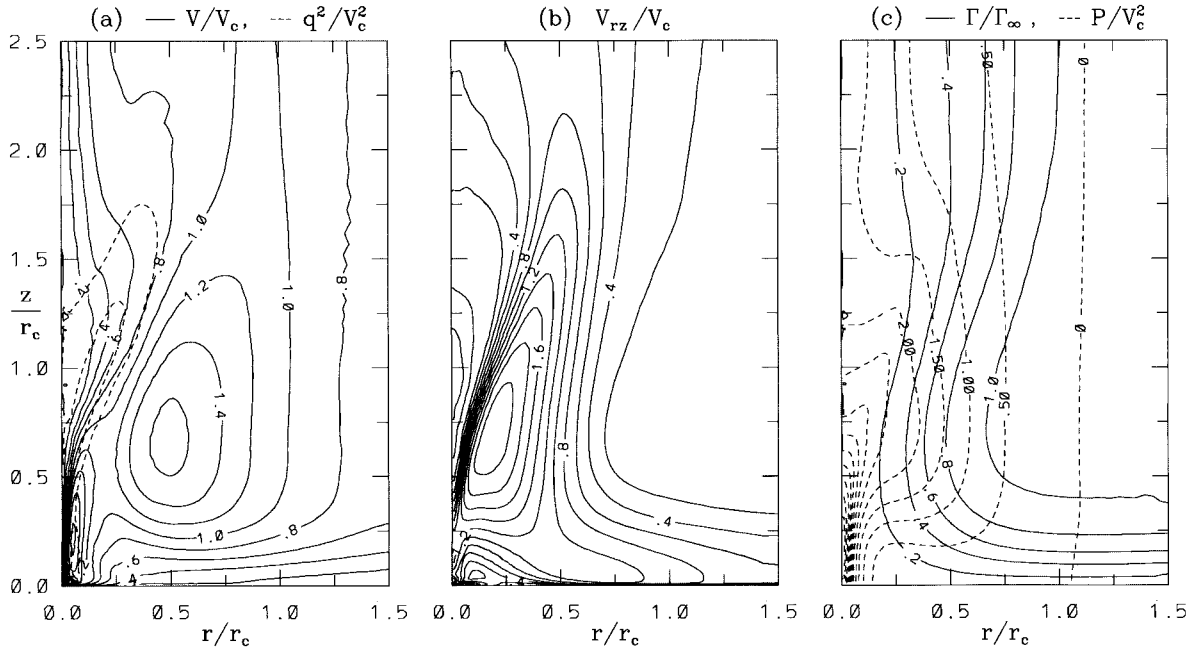

FIG. 15. Normalized, axisymmetric, time-averaged contours in the radial–vertical plane for the simulation discussed in section 4c. (a) Swirl velocity (solid contours) together with highest levels of total velocity variance (dashed, contour level is 0.5), (b) magnitude of the velocity vector in the *r*–*z* plane, (c) perturbation pressure (dashed) and angular momentum (solid).

ure 15 shows the normalized axisymmetric, time-averaged velocity, pressure, and Γ fields for a simulation with boundary conditions as in the case of Fig. 6, but with the zero swirl inflow layer at the outer boundary now only half as thick. In the case of Fig. 6 we found the corner flow overshoot to be small and located well off the surface as is characterized by a very low swirl ratio. In the present case, by reducing the thickness of the zero swirl inflow layer at large radius, Υ has been decreased and S_c correspondingly increased (to 1.4), so that the low-level overshoot is increased toward its maximal value (cf. Fig. 8). This occurs in an interesting fashion, as shown in Fig. 15. There are now two low-level maxima in the swirl velocity within the corner flow—in effect, nested low-swirl corner flows on different length scales. The larger, outer corner flow has its peak swirl velocity occurring where Γ is about 80% of Γ_∞; the inner one, at about 10%. The flat-bottomed vortex breakdown of Fig. 4 is modified here into a conical breakdown. The flow in the breakdown region is highly turbulent (as indicated by the peak turbulent kinetic energy contours in Fig. 15), but is often dominated by a single strong secondary vortex spiraling about the breakdown cone where the velocity gradients are largest.

5. Summary and comments

The qualitative features distinguishing different tornadic corner flows presented here are similar to those exhibited previously in laboratory flows and axisymmetric model simulations by varying the swirl ratio of the large-scale flow. We have added to this qualitative understanding in several ways. First, we have sampled a broader range of boundary conditions for the corner flow, including variations in the surface inflow and upper-core structures, and demonstrated the strong impact they can have on the corner flow structure. Second, we have defined a local corner flow swirl ratio, which incorporates much of the influence of a number of other variables, as well as the outer swirl ratio, on the surface intensification of the tornado. Third, we were able to make the influence of this swirl ratio on the dynamical structure of the flow more quantitative than was previously possible. And finally, we have exhibited the character of the relatively coherent turbulence for different corner flows, which often contributes directly to the greatest damage to structures on the surface. We have not addressed the important question of tornadogenesis on the larger scale, that is, what processes give rise to the converging swirling plume on the few-kilometer scale that is required for a tornado's existence?

The local corner flow swirl ratio, S_c, highlights the role of low angular momentum fluid in the near-surface layer which, upon exiting the boundary layer, forms much of the vertical core flow. It is the radial inertial overshoot of this fluid in the corner flow that provides the chief source of the intensification of swirl velocity and pressure deficit in the mean tornado vortex near the surface. In defining S_c we have utilized only physical properties of the flow field outside of the corner flow that can be robustly measured, for example, whose values are relatively insensitive to the precise radial or vertical position at which they are measured. This new swirl parameter varies directly with the more familiar outer swirl ratio but depends on other parameters as well. It is reduced by anything that increases the surface layer inflow of low angular momentum fluid, such as increases in the effective surface roughness, or the tornado translation speed, or the presence of low-swirl fluid initially below or outside of the larger-scale circulation. It is generally increased by anything that increases the upper-core radius without changing the surface layer inflow, such as the presence of an upper-level central downdraft, or the addition of horizontal divergence in the upper flow. We have found that the effects of such changes on the mean flow structure of the tornadic corner flow are largely quantitatively parameterized by how they change the value of S_c. On the other hand, the magnitude of the outer swirl ratio, S_{outer}, does not by itself categorize the structure of the corner flow if other physical parameters are varied. Flows with the same outer swirl ratio can exhibit quite different corner flow structure.

It should be emphasized that S_c and S_{outer} measure different physical properties of the tornado flow; the former neither replaces nor redefines the latter. While each may be interpreted as the ratio of a characteristic swirl velocity to a characteristic flow through velocity, they are defined on different scales and have different utility. The ratio S_{outer} is a property of the swirling, converging tornado vortex as a whole. As such it represents one of the ingredients (but not the only one) determining the surface layer and upper-core properties of the flow and hence the corner flow structure. The definition of S_{outer} in an open flow necessarily depends on the extent to which the radius and height of the swirling, converging flow are unambiguously defined. The ratio S_c, on the other hand, is a property of the surface layer–core flow embedded within the larger-scale vortex. As such, it can more completely determine the corner flow structure than S_{outer} does but is dependent on, rather than partially determining, the upper-core and surface layer properties outside the corner flow. The S_c is well defined for an unbounded flow as long as there is a strong vortex interacting with a surface.

In section 3, some potentially useful relationships between important tornado dynamical structure parameters were presented as a function of S_c. As S_c decreases, the mean low-level vortex intensity rises to a maximal level; further decrease forces a transition from a very intense low-level tornado vortex to a lower swirl situation with little or no vortex intensification near the surface. Thus the enhancement of low-level, low angular momentum flow may either increase or decrease the tornado intensity depending upon whether it forces the flow toward or below the low-swirl peak intensification point. Mean

swirl velocities close to the surface reach more than 2.5 times the maximum mean swirl velocities aloft under conditions of peak intensification. At very low values of S_c, what little vortex intensification that does occur, occurs well off the surface. This raises the possibility that differences in the near-surface layer inflow may be one of the critical factors determining when or whether an existing kilometer-scale circulation can complete the spinup to a tornado. For a fixed circulation, the intensity of near-surface velocities may not reach levels recognizable as a tornado on the ground if the local corner flow swirl ratio is either too large or too small.

The nature of the coherent, but turbulent, eddy structure is quite different in the various regimes of S_c. Under conditions of peak intensification, there is an unsteadiness in the form of wandering of the narrow central stem of the vortex and in the height of the abrupt breakdown, but most of the large-scale random turbulence remains downstream of the breakdown. At high swirl, the eddies tend to be in the form of secondary vortices rotating around the main vortex in the region of the maximum radial gradients of the vertical and swirl velocities. These eddies are intensified by factors, such as the presence of an upper-level central downdraft, which tend to increase the maximum radial gradients of vertical and/or swirl velocity. In such cases the local intensification within these secondary vortices can be quite large, so that the question of whether low- or high-swirl-type corner flows are the most damaging does not have a simple answer. While S_c provides a useful first-order classification of corner flows, it must be emphasized that, at the level of quantitatively examining the turbulent structure, there is more than just a one-parameter family of possible corner flow behaviors.

To some lowest-order level of approximation, we have reduced the question of the dependence of the corner flow structure on a given physical variable to the dependence of S_c on that variable. We have quantitatively studied the dependence of the corner flow on S_c and qualitatively described the dependence of S_c on a variety of physical variables. A quantitative parameterization of this latter step remains to be presented and is a good candidate for future work.

In this work we have concentrated on the tornado-scale corner flow. It may prove fruitful to apply these results, particularly the definition of S_c, to mesocyclone-scale corner flows in cases where the two corner flows are distinct, for example, when the tornado behaves like a secondary vortex of a high swirl mesocyclone. In recent work, Wakimoto and Liu (1998) have examined the traditional outer-scale swirl ratio for the Garden City, Kansas, mesocyclone in an attempt to understand tornadogenesis in that storm. We expect that the near-surface layer flow will be important in determining the structure of the mesocyclone-scale corner flow, so S_c might prove to be a more useful measure. While it is problematic to obtain radar measurements of the surface layer flow, what we consider the property of the surface layer flow of greatest importance in determining the corner flow structure—namely, the total flux of low angular momentum fluid—can, as we have seen, be measured outside of the surface layer, above the corner flow region.

We should note again that all of the flow patterns exhibited here involve quasi-steady distributions for the particular set of boundary conditions. Accordingly, the applicability of our conditions to real tornadoes is subject to the qualification that the relatively small scale phenomena in the corner flow must remain essentially determined by quasi-steady dynamics as the unsteady outer flow develops. The extent to which the interaction of the tornado with the surface varies, how the local corner flow swirl ratio evolves in time, and whether temporal overshoots are important on some scale, we leave for future work.

Acknowledgments. This research was supported by National Science Foundation Grant 9317599 with S. P. Nelson as technical monitor. We also wish to acknowledge support from the Army Research Office (Grant DAAH04-96-1-0196) in developing the subgrid-scale parameterization incorporating rotational damping given in the appendix, and useful input from the anonymous reviewers.

APPENDIX

Including Some Rotational Damping Effects in an LES Subgrid Model

In a large eddy simulation (LES) one explicitly simulates turbulent eddies large enough to be resolved on the computational grid, and models the effects of eddies that are smaller. If, in a given problem, one can resolve the scales of eddies most important for turbulent transport, then the most important role of the subgrid model is simply to provide an energy sink so that energy does not pile up on the grid scale. In such cases the simulation results should be insensitive to the details of the subgrid model. Sometimes, however, there are regions in a simulation where the larger-scale turbulence is suppressed for some physical reason, and the subgrid contribution becomes relatively more important. Two familiar examples are near a wall, where the scale of the most important eddies is limited by the distance to the wall, and in a stable temperature gradient where the turbulence is damped. One must ensure in these cases that the subgrid model is not overly dissipative, that is, that any physics suppressing the resolved turbulence also suppresses the turbulence represented by the subgrid model. In this appendix we sketch how to include the most important effects of rotational damping within our subgrid model, in analogy with how we have treated the damping in a stratified flow in our LES studies of the planetary boundary layer.

In our subgrid model we carry the subgrid turbulent

kinetic energy as a dynamical variable with evolution equation ($q^2 = 2 \times$ TKE):

$$dq^2/dt + d(u_i q^2)/dx_i = -2\tau_{ij} du_i/dx_j + d(K dq^2/dx_i)/dx_i - q^3/(4\Lambda), \quad \text{(A1)}$$

where

$$\tau_{ij} = -\nu(du_i/dx_j + du_j/dx_i) + \delta_{ij} q^2/3$$

$$K = q\Lambda/3, \qquad \nu = q\Lambda/4 \quad \text{and}$$

$$\Lambda = \min(c_1 \max(\Delta x, \Delta y, \Delta z), 0.65z, 0.5q/N, 0.5q/\xi). \quad \text{(A2)}$$

A sum over repeated indices is assumed. The diagnostic variable Λ should be thought of (up to a constant factor) as the characteristic size of the eddies comprising the subgrid-scale turbulence. In general, we assume that the subgrid turbulence cascades down from the resolved turbulence so that its scale is related to the grid spacing, giving the first term in (A2) (where we typically take $c_1 = 0.25$). The next term in (A2) represents the reduction in eddy length scale as the distance z to the wall becomes small. Note that in this level of approximation the change in scale has been imposed isotropically (there is only a single scale Λ), even though it is only the vertical scale that is directly suppressed due to the proximity of the wall. This is an appropriate treatment within an LES: it is in directions where the resolved scale turbulence is suppressed that the subgrid diffusion might become competitive and hence should be modeled most accurately. In directions where the resolved turbulence is not suppressed, the resolved turbulent transport should dominate the subgrid, so underestimating the latter is of less concern.

The last two terms in (A2) limit the subgrid turbulence length scale in the presence of strong stratification or rotation, respectively. We have patterned the treatment of the latter after the former so we consider the simpler stratified case first. In a region of uniform increasing vertical temperature gradient, dT/dz, a parcel released initially from its equilibrium position with velocity q can (assuming no mixing and the Boussinesq approximation) travel to at most a height $\lambda = q/N$, where $N = \sqrt{(g/T_o)(dT/dz)}$ is the Brunt–Väisälä frequency, before its kinetic energy is all converted into potential energy. An eddy of a given energy in a given temperature gradient is thus limited in vertical extent. This fixes the form of the stratification limit in (A2). The coefficient depends on the ''shape'' of the eddy, its alignment with the gradient, etc., as well as the constant of proportionality between this scale λ and the subgrid turbulence length scale, Λ, as it appears in (A1). We choose the coefficient to match the theoretical critical Richardson number of 0.25 in stratified shear flow.

In a rotating fluid the angular momentum Γ of a small fluid parcel is conserved as it is displaced radially (again assuming no mixing), so that the displacement changes the rotational potential energy in analogy to the change in gravitational potential energy of the vertically displaced parcel in the stratified flow. Given a center of rotation about $r = 0$, a parcel released initially from its equilibrium position with small velocity q directed radially outward in a region of stable rotation gradient, $\Gamma' \equiv d\Gamma/dr > 0$, can travel at most a distance $\lambda = q/\zeta$, where

$$\zeta = \sqrt{2\Gamma\Gamma'/r^3}. \quad \text{(A3)}$$

Assuming the same relation between λ and Λ as in the stratified case, this would give the last limit on Λ in (A2) with $\xi = \zeta$. The rotational damping constraint on the scale is not so easy to implement, however, because in general the center and orientation of the axis of rotation in the flow are unknown a priori; indeed there can be many local centers of rotation that can change position in time (cf. Fig. 2). For ξ, then, we need a local combination of fields that is coordinate invariant, is frame independent (under rotations and Galilean transformations), reproduces (A3) for a purely rotating flow, and does not lead to a strong constraint on Λ for flows (such as uniform shear) without strong streamline curvature. The following choice (written here in Cartesian coordinates for ease of application) fits these conditions:

$$\xi = 2\nabla p \cdot \frac{d\mathbf{V}}{dx_i}\left(\nabla p \cdot \frac{d\mathbf{V}}{dx_i} - \nabla p \cdot \nabla \mathbf{V}_i\right) \Big/ (\nabla p \cdot \nabla p), \quad \text{(A4)}$$

where $\mathbf{V}$ is the velocity vector, p the pressure, and repeated indices are summed. The combination given in (A4) is not unique in fulfilling the required conditions but among the simplest and most local to implement in a finite difference scheme. We note in passing that the stabilizing effects of strong radial temperature gradients within a rotating flow can be included in the same level of approximation by adding the term $-\nabla T \cdot \nabla p/T_o$ to the right-hand side of (A4).

In this implementation of damping effects through the subgrid length scale there is an important feedback mechanism resulting in the subgrid turbulence level being dynamically adjusted to a large degree. In a region of stable rotation gradient, Λ is reduced according to (A2). This causes a reduction of q^2 as given in (A1) that, in turn, further reduces Λ via the q^2 dependence in (A2). Because of this feedback, the effects of employing this subgrid model within our LES has proved to be relatively insensitive to the value of the coefficient in front of the q/ξ term in (A2); when the rotational damping is strong the subgrid diffusion is reduced to where its precise level is unimportant.

We have attempted only to include the first-order effects of rotational damping on the subgrid model in this treatment. We could, for example, also include modifications to the q^2 production terms in (A1) due to the rotation (as we have included subgrid buoyancy production in the treatment of stratification in our boundary layer model). Nonetheless, as implemented it proves beneficial in our tornado simulations: the subgrid tur-

bulence length scale is reduced where it should be, in the main tornado core, and in the cores of the rotating secondary vortices. The corresponding reduction in subgrid diffusion helps to preserve the integrity of the latter, but its biggest practical benefit within our simulations is in reducing the dependence of the upper-core size on the grid spacing there. The turbulent transport of angular momentum radially out of the upper core is a contributing factor in determining the upper-core size. Without the rotational term in (A2), Λ was set by the grid spacing in the upper core and the subgrid transport was unphysically large for coarser grid spacing.

REFERENCES

Burggraf, O. R., and M. R. Foster, 1977: Continuation of breakdown in tornado-like vortices. *J. Fluid Mech.,* **80,** 685–703.

——, K. Stewartson, and R. Belcher, 1971: Boundary layer induced by a potential vortex. *Phys. Fluids,* **14,** 1821–1833.

Church, C. R., J. T. Snow, G. L. Baker, and E. M. Agee, 1979: Characteristics of tornado-like vortices as a function of swirl ratio: A laboratory investigation. *J. Atmos. Sci.,* **36,** 1755–1776.

Davies-Jones, R. P., 1973: The dependence of core radius on swirl ratio in a tornado simulator. *J. Atmos. Sci.,* **30,** 1427–1430.

——, 1986: Tornado dynamics. *Thunderstorms: A Social and Technological Documentary,* E. Kessler, Ed., Vol. II, University of Oklahoma, 197–236.

Fiedler, B. H., 1993: Numerical simulation of axisymmetric tornadogenesis in forced convection. *The Tornado: Its Structure, Dynamics, Prediction, and Hazards,* C. Church et al., Eds., Amer. Geophys. Union, 41–48.

——, and R. Rotunno, 1986: A theory for the maximum windspeed in tornado-like vortices. *J. Atmos. Sci.,* **43,** 2328–2340.

Hall, M. G., 1972: Vortex breakdown. *Annu. Rev. Fluid Mech.,* **4,** 195–218.

Leslie, F. W., 1977: Surface roughness effects on suction vortex formation: A laboratory simulation. *J. Atmos. Sci.,* **34,** 1022–1027.

Lewellen, W. S., 1962: A solution for three-dimensional vortex flows with strong circulation. *J. Fluid Mech.,* **14,** 420–432.

——, 1993: Tornado vortex theory. *The Tornado: Its Structure, Dynamics, Prediction, and Hazards,* C. Church et al., Eds., Amer. Geophys. Union, 19–40.

——, and Y. P. Sheng, 1980: Modeling tornado dynamics. Tech. Rep. NTIS NUREG/CR-2585, U.S. Nuclear Regulatory Commission, 227 pp. [Available from NTIS, Sills Building, 5285 Port Royal Rd., Springfield, VA 22161.]

——, D. C. Lewellen, and R. I. Sykes, 1997: Large-eddy simulation of a tornado's interaction with the surface. *J. Atmos. Sci.,* **54,** 581–605.

Long, R. R., 1958: Vortex motion in a viscous fluid. *J. Meteor.,* **15,** 108–112.

Rott, N., 1958: On the viscous core of a line vortex. *Z. Math. Phys.,* **9,** 543–553.

Shtern, V., and F. Hussain, 1993: Hystersis in a swirling jet as a model tornado. *Phys. Fluids A,* **5,** 2183–2195.

Snow, J. T., 1982: A review of recent advances in tornado vortex dynamics. *Rev. Geophys. Space Phys.,* **20,** 953–964.

Wakimoto, R. M., and C. Liu, 1998: The Garden City, Kansas, storm during VORTEX 95. Part II: The wall cloud and tornado. *Mon. Wea. Rev.,* **126,** 393–408.

Ward, N. B., 1972: The exploration of certain features of tornado dynamics using a laboratory model. *J. Atmos. Sci.,* **29,** 1149–1204.

Wilson, T., and R. Rotunno, 1986: Numerical simulation of a laminar end-wall vortex and boundary layer. *Phys. Fluids,* **29,** 3993–4005.